ilmedia

TECHNISCHE UNIVERSITÄT
ILMENAU

Song, Xinya; Cai, Hui; Jiang, Teng; Sennewald, Tom; Kircheis, Jan;
Schlegel, Steffen; Noris Martinez, Leonel; Benzetta, Youcef; Westermann, Dirk:

Research on performance of real-time simulation based on inverter-dominated power grid

Original published in:	IEEE access / Institute of Electrical and Electronics Engineers. - New York, NY : IEEE. - 9 (2021), p. 1137-1153.
Original published:	2020-08-12
ISSN:	2169-3536
DOI:	10.1109/ACCESS.2020.3016177
[*Visited:*	2021-02-22]

This work is licensed under a Creative Commons Attribution 4.0 International license. To view a copy of this license, visit https://creativecommons.org/licenses/by/4.0/

TU Ilmenau | Universitätsbibliothek | ilmedia, 2021
http://www.tu-ilmenau.de/ilmedia

Received July 6, 2020, accepted August 5, 2020, date of publication August 12, 2020,
date of current version January 5, 2021.

Digital Object Identifier 10.1109/ACCESS.2020.3016177

Research on Performance of Real-Time Simulation Based on Inverter-Dominated Power Grid

XINYA SONG[1], (Member, IEEE), HUI CAI[1], (Member, IEEE), TENG JIANG[1], (Member, IEEE), TOM SENNEWALD[1], (Member, IEEE), JAN KIRCHEIS[1], (Student Member, IEEE), STEFFEN SCHLEGEL[1], (Member, IEEE), LEONEL NORIS MARTINEZ[2], (Member, IEEE), YOUCEF BENZETTA[2], AND DIRK WESTERMANN[1], (Senior Member, IEEE)

[1]Department of Power System, Technische Universität Ilmenau, 98693 Ilmenau, Germany
[2]OPAL-RT Technologies, France

Corresponding author: Xinya Song (song.xinya@tu-ilmenau.de)

This work was supported for the Article Processing Charge by the Open Access Publication Fund of the Technische Universität Ilmenau.

ABSTRACT This paper proposes two methods to improve the performance in real-time simulation. The increased inverter-based generations are gradually shifting the operation of the power grid. Consequently, the investigation for the safe operation and further application is essential in the inverter-dominated power grid. As the simulated number of non-linear switch elements like inverter increases, the numerical complexity of the simulation model rises exponentially. Accordingly, the scale of the simulated power grid with inverters is normally constricted by taking account of the burdensome numerical calculation. The emerging of real-time simulator provides the opportunity to enable the simulation of the large-scale power grids. Nevertheless, the simulation boundary condition is still exceeded in the inverter-dominated model. Hence, the improvement of the performance to extend the limitation in real-time simulation is constituted in this paper. The first method proposed is co-simulation. This approach is to simulate the power grid and inverters by models in different deep levels. The phasor model and electrical-mechanical-transient model are utilized to develop the co-simulation model. The second method is network reduction. Based on the dynamic feature of the inverter, it is reduced to an equivalent current source, which decreases the complexity of the model and retains its characteristics. The evaluation of the methods is demonstrated by two indexes: real-time capability and the similarity degree.

INDEX TERMS Real-time simulation, inverter-dominated power grid, co-simulation, network reduction.

I. INTRODUCTION

The increasing number of power electronic based devices, such as photovoltaic, wind generation device and HVDC is interfaced with the power grid [1]–[4]. This trend means that conventional power plants are gradually being switched off and the deployment of renewable energies is growing [2]. Feeding renewable energy into the power system is mainly implemented in the distribution grid, and the conversion system plays a significant role, which can lead to the reduction of inertia of power system with the expending of the renewable feed-in-power [5]–[7]. Due to the inherent quick switching characteristic and non-linear nature of electronic-based controllers, these power electronic semiconductors in the conversion system have brought challenges to the stable operation of the power grid [3]–[5]. On the one hand, the volatility of renewable energy could cause system-wide instability; on the other hand, the non-linear characteristic of the semiconductor elements often leads to power quality problems and various interactions of different application areas [7], [8]. Furthermore, the power injections from renewable energy are distributed. The parallel operation of converters could cause interactions between device controllers, such as coupled oscillations [8], [9]. This oscillation can transmit to the high voltage level and expand to the low voltage level on account of the reduction of inertia of power network, which is because of the increased ratio of renewable energies and the decreased number of conventional power plants. Thus,

The associate editor coordinating the review of this manuscript and approving it for publication was N. Prabaharan.

This work is licensed under a Creative Commons Attribution 4.0 License. For more information, see https://creativecommons.org/licenses/by/4.0/

potential problems in the future power grid should be investigated [7], [9], especially the network with a large amount of distributed generations.

However, on account of the numerical difficulty, the traditional offline simulation has usually a limitation with the large-scale power grid by detailed equivalent model (DEM) and average value model (AVM), which usually needs a large amount of time to execute the simulation [8]–[12]. Especially, with the increasing number of components, the expanding of the scale and the complexity of power network, the problems like the simulation time consumption, convergence error and iteration fault can gradually emerge [12]–[14]. The more detailed the model is, the more problems will appear. Besides, there are, nowadays, more and more requirements to simulate with the real hardware, because the simulation results of it could be more closed to the reality [15]. The real-time simulation will be accordingly more used with the increasing demands. With the real-time simulation, more applications can be implemented such as the investigation between the hardware and the simulation can be applied through the hardware-in-the-loop simulation (HIL) and rapid-control-prototyping (RCP) [15], [16]. Meanwhile, with its powerful computing ability, the investigation of a large-scale power grid in DEM and AVM can be taken into account.

The real-time simulator OPAL-RT is applied in this paper to execute the real-time simulation of power grid with different levels of the inverter [15]–[17]. With the growing number of inverters, the calculation time of simulation is correspondingly growing up, which can reach to the limitation to guarantee the real-time operation. However, there are two ways to accelerate the calculation: Firstly, the main calculation system can be divided into different subsystems, which can perform the computation simultaneously. It is also called parallel computing [18]. Although the calculation can be accelerated, it is extremely dependent on the core of real-time simulator, namely the core of real-time simulator. The simulator in this work has four cores, which means that the calculation can be divided into four subsystems to execute parallel computing. Another way is to apply the acceleration elements into the simulation. In supported elements from OPAL-RT library, the toolbox ARTEMiS can be utilized into the acceleration. By application of Distributed Parameter Line (DPL) from the toolbox, the transmitted signals can be decoupled into the smaller matrices, which could accelerate the calculation. Despite these, the boundary condition can still be reached up with the increasing of DEM or AVM models. Accordingly, this work provides another two methods which serve as the extended ways to accelerate the simulation. The idea of the first method is derived from the co-simulation [20]. The co-simulation is through combining DEM or AVM with the phasor model (PM) to build a hybrid model that takes both advantages of them that we can observe the dynamic behavior from DEM or AVM detailly, and the execution speed of PM is faster [21]–[23]. The simulation blocks ePHASORSIM and eMEGASIM from OPAL-RT can respectively simulate the large scale over layer power network in phasor domain and in EMT based detailed equivalent model [15]. The other method is applied to accelerate the real-time simulation by means of network reduction [24] with the aggregated model. With the network reduction procedure, the structure of complicated power network can be simplified without distorting the characteristics and the dynamic behaviour of the original system. After that, the consideration is given to the comparison of dynamic state between the original power network and the reduced model, which is presented in the evaluation of the model at the end of the paper.

To explain the above-mentioned methods, this article can be organized as follows: The chapter II provides a brief overview of three models in different levels in power system. The numerical calculation process of these models is expounded in this chapter. Afterward, the investigation of the boundary condition with the presented real-time simulator is illustrated in chapter III. Besides, there exist two methods: parallel computing and the acceleration component from the RT-LAB library as the expanding the boundary of real-time simulation. They still have the limitation, which is also shown in this chapter. In chapter IV, the two novel methods: co-simulation and network reduction, are illustrated for further expanding the boundary of real-time simulation. The evaluation of these two methods is presented in chapter V. Finally, the paper is summarized in chapter VI.

II. MULTI-LEVEL MODELING OF INVERTER

The simulation is the essential part of the planning, designing, and operating of a power network. The required model is always depending on its application. With consideration of different application, the models in different levels can be applied to simulation. Generally, Fig.1 categorizes the electrical power network models into the following four different levels: architecture level, functional level, behavioral level, and component level [8], [14], [26], [27]. The model in the top architecture level has the smallest complexity and is used for the steady-state network analysis, e.g. power flow calculation

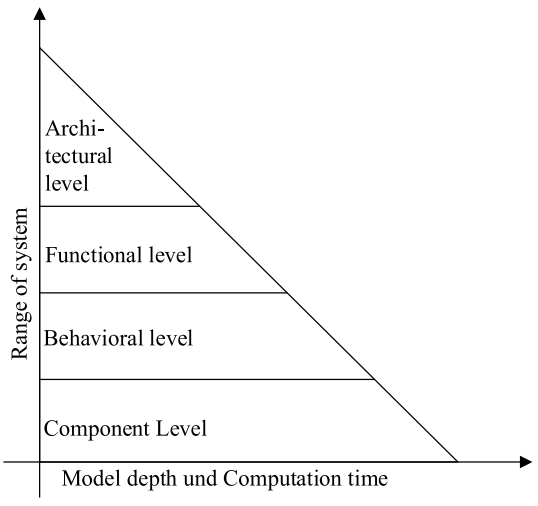

FIGURE 1. Multi-level modeling paradigm [8].

and network planning. The next level is generally known as the functional level by which high-frequency behavior up to 150Hz can be described. Both the modeling frequency and the complexity of a functional-level model are increased compared to the top level, which in turn supports a fundamental harmonics analysis of steady-state and the slow electromechanical transients in a large power system [9], [12]. Nowadays, functional models are frequently used for the modeling of electrical power converters, such as the average value model [8] and the phasor model [14]. Models in the next two levels are presented in more detail. The model in the behavioral level uses lumped-parameter subsystem models and the modeling frequencies can be up to hundreds of kHz [8]. Models in this level cover the switching behavior and the impact of harmonics. The modeling frequencies can be up to the MHz region if required [26]. All components are modeled in detail and the instantaneous quantities are used for simulation. Using these models, network behaviors, such as harmonic and fast electromagnetic transients (EMT), can be simulated. The electrical power model in this level is known as DEM. Under the traditional simulation environment, the models in the behavioral level such as AVM and in the component level like DEM, with which we can observe the power network in a deeper view. In this chapter, the three mentioned models (DEM, AVM and PM) are discussed in more detail below.

A. DEM

The detailed model is constructed based on the true physical structure of an inverter, i.e. each component in an inverter is considered. Since the nonlinear switching characteristic of the semiconductor elements and the pulsed working behavior can be described, simulations with detailed models are accurate [8], [9].

This model is well suited to performing harmonic and EMT studies. Depending on the application, the detailed model has simplified variants, which have relatively low modeling frequencies, like on the behavioral level [9]. However, the detailed model is time-inefficient for the simulation of a large power system because of its high modeling frequency and a large amount of data. To solve this problem, time-efficient models have been developed.

B. AVM

Compared to the detailed model, the average value model has reduced complexity with average switching behavior and circuit behavior over each switching period [28]. The average value is calculated from the below equation (1)

$$\bar{U}_{A0} = \frac{1}{T_p} \int_{t}^{t+T_p} U_{out}(t)dt \tag{1}$$

As shown in Fig.2, the variety of the magnitude within a switching period is reduced and partially compensated by using average values. Since the behavior of this model is no longer pulsed, a significant increase in simulation time is achieved. Assuming that DC voltage remains constant,

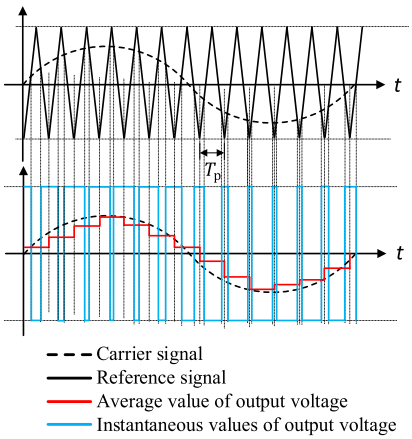

FIGURE 2. Comparison between DEM and AVM.

the average value of a period in case of a sufficiently high pulse frequency would be approximated to a reference waveform. The output AC voltage is performed ideal sinusoidally and the switching dynamics are disregarded. Therefore, the circuit bridge can be modeled as controlled voltage sources [29].

The averaged model can be used to characterize steady-state operation, electromechanical transient behavior, and DC link dynamics. This modeling technique has been widely used to study power converters [12] and has numerous variants as shown in reference [8], [12] and [28]. But the efficiency of the AVM decreases dramatically when a power system is under unbalanced conditions [12]. The main reason is that the variable transformed in the dq-coordinate is no longer constant, due to the negative sequence component which will become the second harmonic in the dq-coordinate. The simulation speed is thus decreased [12], [28]. As an alternative approach, the phasor model, also referred as the general averaging model has been developed [29].

The averaged model can be used to characterize steady-state operation and electromechanical transient behavior and DC link dynamics. This modeling technique has been widely used to study power converters [12] and also has numerous variants as shown in reference [8], [12] and [28]. But the efficiency of the AVM decreases dramatically when a power system is under unbalanced conditions [12]. The main reason is that, the variable transformed in the dq-coordinate is no longer constant, due to the negative sequence component which will become the second harmonic in the dq-coordinate. The simulation speed is thus decreased [12], [28]. As an alternative approach, the phasor model, also referred as the general averaging model has been developed [29].

C. PM

Some power system analyses are only interested in magnitude and phase angle of currents and voltages changing in slow oscillation modes after disturbances. In such analyses, the currents and voltages will be computed as phasors. That is, the sinusoidal voltages and currents are replaced with

complex numbers to represent their magnitudes and phase angles at a particular frequency:

$$x = Re\left\{(Xe^{j\theta}) \cdot e^{j\omega t}\right\} \triangleq X\angle\theta \tag{2}$$

The root-mean-square value instead of the peak value is used in phasors. Using the phasor model, capacitances (C) and inductances (L) are described by their complex algebraic equations. The fast oscillation modes (in the differential equations form) between L and C are therefore ignored [28]. In the phasor model, the inverter bridge circuit is the same as in AVM, which is modeled as a controlled three-phase AC voltage source. Based on the assumption that only fundamental frequency will be considered, the results of PM correspond to the perimeter of the results of AVM under the same conditions (see Fig.3). Since the variations of phasor values are much slower than the instantaneous ones, simulation is faster than AVM.

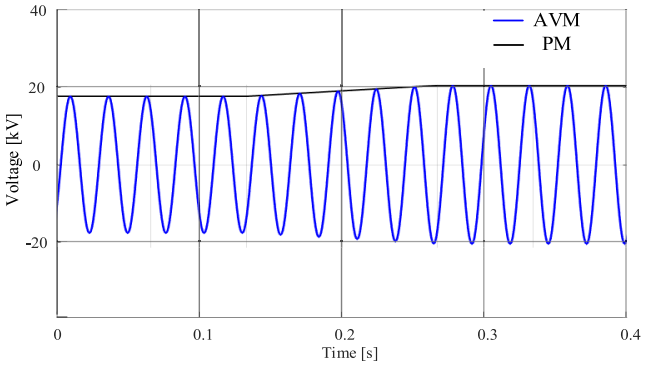

FIGURE 3. Comparison between PM and AVM.

III. THE BOUNDARY INVESTIGATION OF REAL-TIME SIMULATION

OPAL-RT simulator provides four simulation systems to satisfy the different applications, which depend on the size and the simulation interval of the model. Two simulation systems will be applied in this research: eMEGASIM and ePHASORSIM. These two systems correspond to the different time range. eMEGASIM offers a direct platform compatible with ePHASORSIM, which procure maximum versatility from a large power grid simulation to highly detailed power electronic simulation. ePHASORSIM allows the simulation of massive grids going up to 20k buses on a single core computer and its capability to perform parallel computing allowing unleashed performances for lager real-time simulation [30]–[33], [38]. The typical time step of these two systems is displayed by Fig.4.

A 20-kV distribution grid is modeled aligning Cigré benchmark [29], which is utilized as the basic model to apply in the investigation. Both feeders of the open ring topology operate at 20 kV and are fed via separate transformers from the 110 kV sub-transmission systems, which is a typical form of medium-voltage networks in Europe see Fig.5.

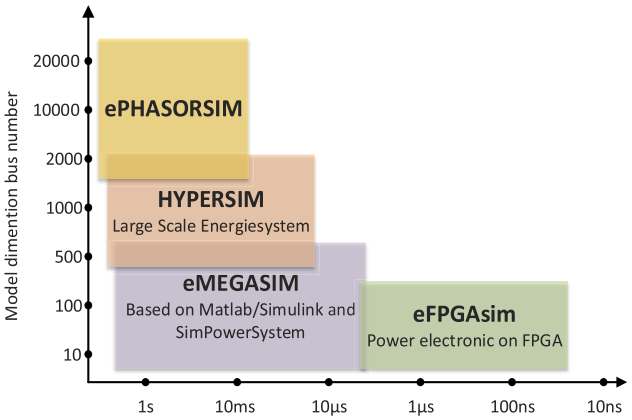

FIGURE 4. Spectrum of the simulation systems in OPAL-RT [18], [19].

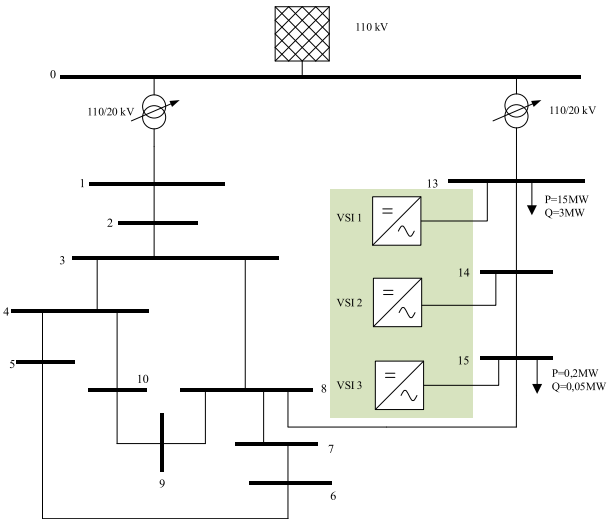

FIGURE 5. Simulation test grid, cf. [19].

The 20 kV Grid includes 16 buses, three of them are active buses, at which the inverter models are connected. The inverter consists of an I-control-loop, a U-control-loop, and an upper-level reactive power controller for the voltage support. Fig.6 has compared the performance of three models for inverters in DEM, AVM, and PM according to the events in TABLE 1.

TABLE 1. Simulation scenario of grid-connected mode.

Scenario						
		P [MW]			PF	U_g [P.U.]
Initial state		VSI 1	VSI 2	VSI 3	0.95	1
		4.75	4.75	4.75		
From	to					
0	0.1	4.75	4.75	4.75		1
0.1	0.2	3	3	2		1
0.2	0.3	4.75	4.75	4.75		1

Fig. 6 illustrates the topology of the inverter circuit, which connects with the voltage source of the grid. The circuit is

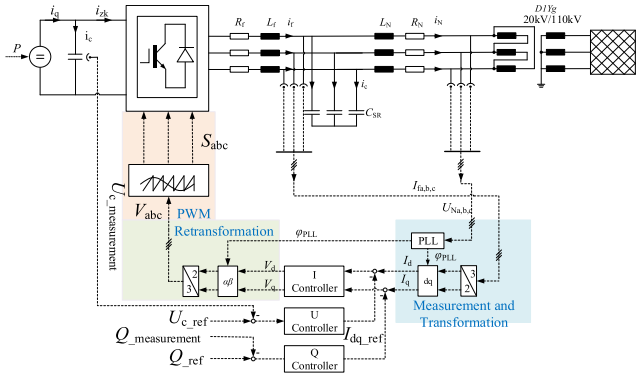

FIGURE 6. The topology of inverter and the control loop.

shown in natural coordinates, which includes a three-phase inverter with an intermediate voltage circuit, filter circle, grid network connected with the Dy 20/110kV transformer and the overlaid control loops including the voltage, reactive power and the current control loop. PLL is used to synchronize the phase with the grid in the transformation. To model the dynamic process by using the differential equations, the system behaviour is first converted to vector coordinates ($\alpha\beta$ coordinates).

In circle I and II of Fig.7:

$$\begin{cases} \underline{\vec{u}}_{\mathrm{n}} = L_{\mathrm{N}} \cdot \dfrac{d}{dt}\underline{\vec{i}}_{\mathrm{N}} + R_{\mathrm{N}} \cdot \underline{\vec{i}}_{\mathrm{N}} + \underline{\vec{u}}_{\mathrm{c}} \\ -\underline{\vec{u}}_{\mathrm{c}} = L_{\mathrm{f}} \cdot \dfrac{d}{dt}\underline{\vec{i}}_{\mathrm{f}} + R_{\mathrm{f}} \cdot \underline{\vec{i}}_{\mathrm{f}} - \underline{\vec{u}}_{\mathrm{SR}} \\ \underline{\vec{i}}_{\mathrm{N}} + \underline{\vec{i}}_{\mathrm{f}} - \underline{\vec{i}}_{\mathrm{c}} = 0 \\ \dfrac{d}{dt}\underline{\vec{u}}_{\mathrm{c}} = \dfrac{\vec{i}_{c}}{C_{\mathrm{SR}}} \end{cases} \tag{3}$$

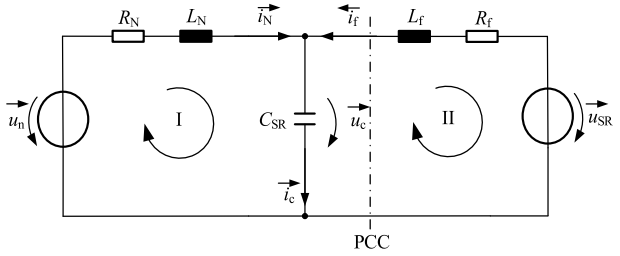

FIGURE 7. Equivalent circuit diagram of inverter and power network in $\alpha\beta$ coordinate.

The $\underline{\vec{u}}_{\mathrm{n}}$ and $\underline{\vec{u}}_{\mathrm{SR}}$ are the voltage of grid and inverter in a vector coordinate, $\underline{\vec{u}}_{\mathrm{c}}$ is the voltage of capacitor. The $\underline{\vec{i}}_{\mathrm{N}}$, $\underline{\vec{i}}_{\mathrm{f}}$ and $\underline{\vec{i}}_{\mathrm{c}}$ are the current of the power grid, inverter and capacitor. L_{N}, R_{N} and L_{f}, R_{f} are the inductance and resistance of network and filter circle. C_{SR} is the capacitor in the filter circle.

The state variables are controlled to ensure the normal operation of power inverters [27]. In order to maintain the current and voltage at the operation point, the controller is designed to eliminate the malfunctions that prevent the inverter from operating. In general, the control concept is presented according to the topology in Fig.6. Two controllers are implemented: an overlaid voltage controller for the stabilizing the DC link voltage and an underlaid current controller for filtering current.

It can be shown that the responses from all the three models are in close agreement with each other, particularly in steady states, see Fig.8. Obviously, the validations of the three inverter models are verified. Besides, the accuracy is also in line with our expectation (the errors of models are less than 5% compared with each other under static conditions). Due to the consideration of the switching, the ripple of the output voltage in DEM is pulsed. This distorted voltage contains the fundamental frequency component as well as the high-frequency components. Conversely, only the fundamental frequency is presented in AVM and PM as the switching behaviors are neglected. PM only gives magnitude, which also matches well. In addition, the network operation in PM is described by complex algebraic equations. This makes the phasor model directly react to a disturbance. Fig. 8 shows the simulation results of the output voltages of the inverters, which amplitude is $\frac{\sqrt{2}}{\sqrt{3}} \cdot 20kV = 16.3kV$. Because of the switching mode of operation in DEM, the waveforms of the output voltages (red line in Fig. 6) show a pulsed signal.

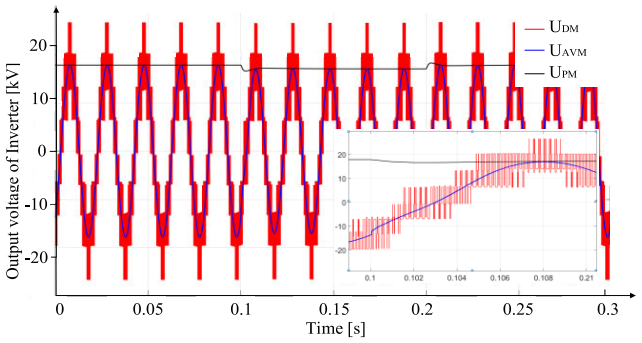

FIGURE 8. Comparison of simulation results at changing of an operating point: A phase output voltage of the corresponding inverter.

This distorted voltage contains the high-frequency component in addition to the fundamental frequency component. By contrast, in AVM and PM, only the fundamental frequency component is presented because the switch behaviors are ignored. The voltage curves are completely adjusted here. While the output voltages of the inverter in AVM (blue line in Fig. 8) are ideally sinusoidal, the phase model considers only the peak value and the phase angle. The phase angle is not marked in Fig.8. With eMEGASIM, the data stream will be first calculated in CPU and then executed in the FPGA for coordinating and cooperating with the I/O ports. RT-LAB is the platform offered by OPAL-RT, where the model can be programmed and simulated under eMEGASIM [39]–[41]. Fig. 9 shows the procedure to run the real-time simulation.

A. INVESTIGATION OF BOUNDARY CONDITION OF eMEGASIM

The model is initially applied in one calculation system without any acceleration method (see Fig.10). As is shown in

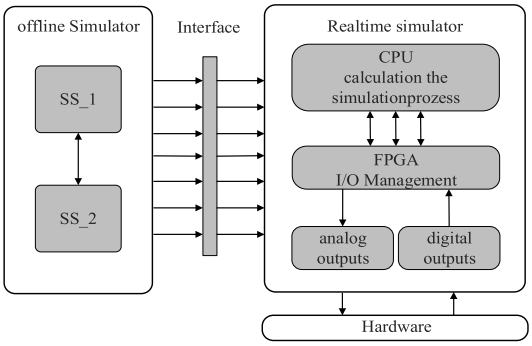

FIGURE 9. The process of the real-time simulation.

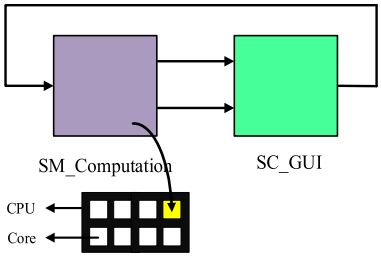

FIGURE 10. The process of the real-time simulation.

the figure, the subsystems have originally two parts: computation subsystem and graphic user interface (GUI) subsystem, which are separately named as SM_Computation (Slaver master) subsystem and SC_GUI (Slaver console). The computation subsystem is responsible for the numerical calculation for the simulation. GUI subsystem aims to show the results of the simulation [34]–[37]. The number of the computing subsystem is in correspondence with the quantity of the applied core in CPU. The investigation of boundary condition of eMEGASIM proceeds in one core. The simulation results are illustrated in TABLE 2.

TABLE 2. Running time of different models in real-time simulation.

Model	System	Inverter number	Interval [μs]	Usage-value [%]	Running time [μs]
DEM	1	3	200	96	192
		4		Overrun	Overrun
AVM	1	3	50	90	45
		4		98.3	49.25
		5		Overrun	Overrun
PM	1	3	50	70.7	35.35
		4		78.9	39.45
		6		94	47
		7		Overrun	Overrun

From the table, it is illustrated that the simulation DEM in one core, which has three inverters and needs 192μs. It occupies 96% usage of the core. But the AVM and PM, with the same inverter number, take less time and the usage of core to finish the calculation. The boundary condition of using eMEGASIM in one calculation system is that a maximum 3 DEM inverters with 200μs interval can be applied in real-time simulation. In comparison with the other two model types, the boundary conditions are: maximum 4 AVM inverter and 6 PM inverter with 50μs can be implemented in one core for the real-time simulation, otherwise the simulation overruns. To expand the boundary condition, OPAL-RT has provided two usually utilized methods: parallel computing and the ARTEMiS.

B. SOLUTION FOR EXTENDING THE BOUNDARY CONDITION

Parallel computing reduces calculation consumption by distributing the calculation task on several cores of one CPU. All cores can execute the simulation simultaneously [32], [36]. It is designed in real-time simulator for processing large amounts of data. The central idea of applying this method is to divide the entire model into several subsystems. The number of cores in CPU limits the maximum number of subsystems.

Fig. 11(a) presents the computation without using parallel computing, which means that one core in CPU is used in simulation. In Fig 11(b), the system is divided into two subsystems. Each one owns a core to execute the calculation at the same time. In this research, we use the OP5600 as our simulator and it has four cores in CPU.

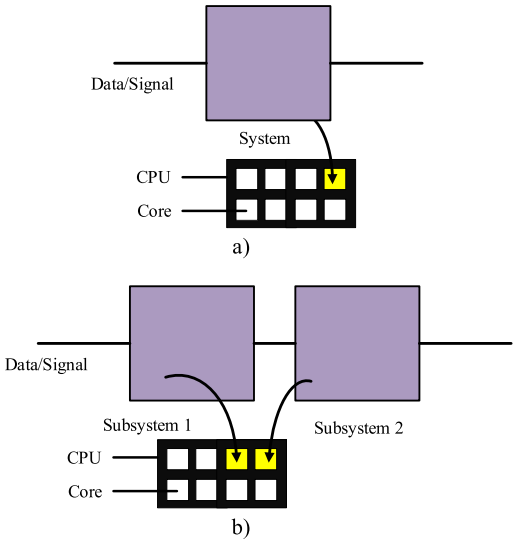

FIGURE 11. The concept of parallel computing.

The system can be one subsystem or split into two or four calculation subsystems. Fig. 12 shows the arrangement of a four-subsystem topology.

The second acceleration method is using the ARTEMiS block. ARTEMiS provide available decoupling methods to reduce the complexity of the model, such as SSN (state-space-nodal), ARTEMiS DPL, and Stubline. These decoupling methods are used for single-core and multi-core simulation. The block divides the large state space equation (3) into several smaller state-space matrices with replacing C_1, C_2, D_1, D_2 by 0. Accordingly, it reduces the size of

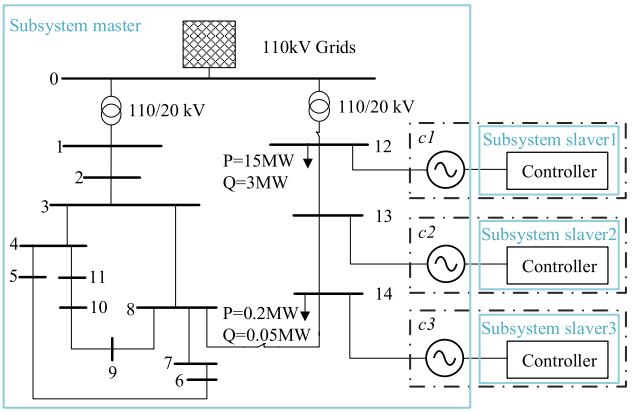

FIGURE 12. Topology of simulation model with parallel computing.

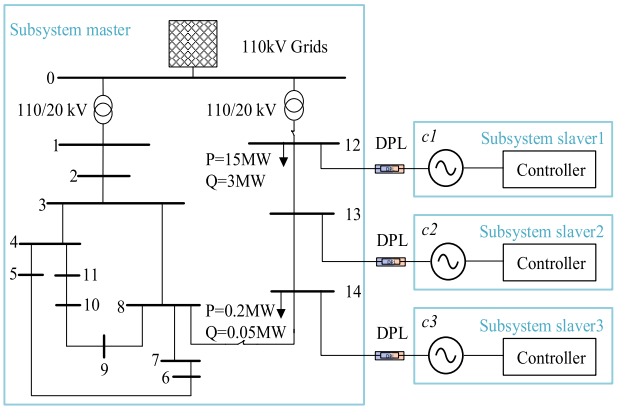

FIGURE 13. Topology of simulation model with ARTEMiS DPL.

the matrix, which thereby makes the calculation faster.

$$x_{n+1} = \begin{bmatrix} A_1^m & C_1 \\ C_2 & A_2^n \end{bmatrix} x_n + \begin{bmatrix} B_1^m & D_1 \\ D_2 & B_2^n \end{bmatrix} u_n \tag{4}$$

The simulation uses physical-based lines and connectors to model the power grid. The signals cannot be used to communicate between subsystems in OPAL-RT real-time simulation. The insertion of ARTEMiS DPL at the root level of the block diagram allows connection to the physical modelling ports of the block with the real-time subsystems [35]. By using it, the inverter can be separated from the system independently as one subsystem. The results of the two presented acceleration methods are shown in the following table. For ARTEMiS block, it can only be implemented in the AVM. ARTEMiS cannot work in PM because it must be under the discrete-time environment. In PM, the simulation environments are phasors and the amplitude. ARTEMiS cannot work in DEM, because three-level bridge block is used in the DEM-based inverter. There are 18 switches in it, which can lead to the memory overflow in the calculation of switching matrix permutations. In this paper, ARTEMIS DPL has been used to replace normal distributed parameter line. It has two functions; one is to directly accelerate the simulation. The other is that, because of the replacement of distributed parameter line, the inverter can be separated as one subsystem slaver. It helps to combine the parallel computing and the implementation of ARTEMIS together.

Fig.13 shows the topology of a four-subsystem with three ARTEMiS DPL. The real-simulation time comprises calculation time in CPU and command time in FPGA. When this running time is smaller than a predetermined time interval, it is real-time capable. When the running time is greater than the time interval, the interval can be extended to achieve real-time capability. With acceleration methods, the calculation time can be reduced. Thereby the running time is reduced. The usage value of the core provides information about the real-time capability. If usage value is below 100%, the simulation is running in real-time. Otherwise, there is an overrun. Overrun in the simulation cause highly biased results. Also, the behavior of the system becomes uncertain.

TABLE 3 shows the calculation time of three model types with three scenarios of parallel computing. The number of subsystems, different time intervals, the usage value, and the calculation time are shown in this table. From the table, it is illustrated that the maximal simulated number of inverters by DEM is five with using four cores through parallel computing. The usage of simulator reaches 98% by simulating four DEM inverters. While the maximal number of simulated AVM inverters can reach up to ten. The usage of four cores by simulating ten inverters is 96.7%.

TABLE 3. Real-time capability with parallel computing.

Model	System	Inverter number	Interval [μs]	Usage-value [%]	Running time [μs]
DEM	1	3	200	96	192
	2	3	200	89	178
	4	3	200	87	174
	4	5	200	98	196
AVM	1	3	50	90	45
	2	3	50	75.98	37.99
	4	5	50	40.62	20.31
	4	10	50	96.7	48.35
PM	1	3	50	70.7	35.35
	2	3	50	38.7	19.35
	4	3	50	22.9	11.45
	4	14	50	97	48.5

As another acceleration method ARTEMiS, the DEM and PM are not suitable to be applied. Accordingly, the investigation of the boundary condition for ARTEMiS with parallel computing is executed with AVM. TABLE 4 shows the calculation time of AVM with the different number of ARTEMiS blocks in one, two and four subsystems.

The number of DPL, the time interval, the usage value, and the calculation time are shown in this table. It shows that the implementation of DPL can significantly decrease the usage value. By using three DPL, the usage value of one core to simulate three AVM inverter reduces from 90% to 52.88%. With implementation the parallel computing, the minimal usage value can reach up to 21.21%, which means that more AVM inverters can be simulated in real-time simulator.

TABLE 4. Real-time capability with ARTEMiS DPL.

Model type	Numbers of subsystems	Numbers of DPL	Time interval [µs]	Usage-value [%]	Running time [µs]
AVM	1	0	50	90	45
		1	50	63.47	31.74
		2	50	57.28	28.64
		3	50	52.88	26.44
	2	0	50	75.98	37.99
		1	50	45.47	22.74
		2	50	41.88	20.94
		3	50	37.45	18.73
	4	0	50	40.62	20.31
		1	50	26.35	13.18
		2	50	23.85	11.93
		3	50	21.21	10.61

IV. CO-SIMULATION AND NETWORK REDUCTION

Although the simulation speed can be accelerated through parallel computing and ARTEMiS toolbox, the boundary of real-time simulation still exists. When the bus number of model reach to thousand and the number of inverter models rises to hundred, the AVM and DEM are not suitable to be simulated by eMEGASIM anymore. In this chapter, two new methods are able to further expand the boundary condition of using eMEGASIM: Co-simulation and network reduction.

A. CO-SIMULATION

The realization of the co-simulation is by using an equivalent model through boundary conditions between two models. One of the models is needed to be substituted. The feasible method is to replace the model with an ideal voltage or current source. The drawback of this method is that it neglects the current or voltage change in conjunction bus [20]–[22]. Another method is to replace the EMT subsystem with a current source and the PM subsystem with a current source parallel to a frequency-dependent network equivalent (FDNE) admittance [21]. The method produces results with higher accuracy especially with large frequency changes if the system is disturbed [22], [42], [44].

In general, the process of the combination of PM subsystem und EMT subsystem is illustrated in Fig.14. The co-simulation model consists of AVM and the PM. Through the Thevenin equations in PM system, the variable voltage $U\angle\varphi$ is sent to the EMT subsystem as input. After calculation in EMT subsystem, the current as the output of EMT subsystem is transferred to PM subsystem. The further investigation about it will be reported in the following part 1) and 2).

1) FROM PM TO EMT THROUGH TIME INTERPOLATION

Through the time interpolation, the voltages and currents of PM form can be transformed to EMT form with the smaller time step. In time interval $t \in [t, t+H]$, the voltage can be calculated by Thevenin equation at time $t+H$ as follows:

$$\bar{E}_{pm}(t+H) = \bar{V}^{k+\frac{1}{2}}(t+H) - Z_{pm} I^{k+\frac{1}{2}}(t+H) \quad (5)$$

The large time step H is a multiple of the small-time step h or $H = ph$ with $p \in \mathbb{N}$. The interpolated voltage magnitude

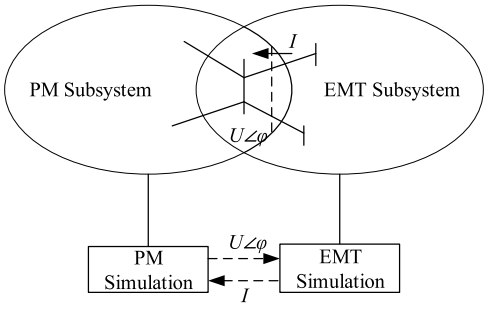

FIGURE 14. Interaction between PM and EMT solver [20].

at time $t+mh$ $(m = 0, \ldots, p)$ is defined as follows:

$$\left\|\bar{E}_{pm}(t+mh)\right\| = \left\|\bar{E}_{pm}(t)\right\| + \frac{m}{p}\left(\left\|\bar{E}_{pm}(t+H)\right\| - \left\|\bar{E}_{pm}(t)\right\|\right) \quad (6)$$

Consequently, the voltage Thevenin equation in EMT form can be calculated out in three-phase:

$$e_{abc}(t+mh) = \sqrt{2}\left\|\bar{E}_{pm}(t+mh)\right\| \cos(\omega_s\left(t+mh \pm \frac{2\pi}{3}\right) + \angle\bar{E}_{pm}\left(t+mh \pm \frac{2\pi}{3}\right)) \quad (7)$$

e_{abc} : AC voltage, $\left\|\bar{E}_{pm}\right\|$: Amplitude of PM voltage $\angle\bar{E}_{pm}$: Angle of PM voltage

2) FROM EMT TO PM THROUGH THE PHASOR EXTRACTION

This process will use the three-phase current signals in EMT system. Firstly, the current will be projected into dq axis, which is applied in PLL [16]. With the transformation matrix:

$$T = \frac{\sqrt{2}}{3}\begin{bmatrix} \cos\theta & \cos(\theta - 2\pi/3) & \cos(\theta - 4\pi/3) \\ -\sin\theta & -\sin(\theta - 2\pi/3) & -\sin(\theta - 4\pi/3) \end{bmatrix}$$

$$i_{abc} = \begin{bmatrix} i_a \\ i_b \\ i_c \end{bmatrix} = \sqrt{2}\, I_a \begin{bmatrix} \cos(\omega_s t + \varphi_a) \\ \cos(\omega_s t + \varphi_a - 2\pi/3) \\ \cos(\omega_s t + \varphi_a - 4\pi/3) \end{bmatrix} \quad (8)$$

It follows:

$$i_{xy} = \begin{bmatrix} i_x \\ i_y \end{bmatrix} = I_a \begin{bmatrix} \cos\varphi_a \\ \sin\varphi_a \end{bmatrix} \quad (9)$$

With the magnitude $I_a = \sqrt{I_x^2 + I_y^2}$ and phase $\varphi_a = \arctan(I_x / I_y)$. This form is the representation of PM. i_{xy}: The vector of instantaneous components on the xy axes.

To investigate the dynamic characteristic of the co-simulation model, a 20kV distribution grid is modeled aligning Cigré benchmark [29] To investigate the dynamic characters of a hybrid model, the above medium-voltage network with parallel switching of three VSI will be divided into two parts: first is the grid, which will be simulated by ePHASORSIM and the second part is the inverter, which will be implemented in the eMEGASIM that can simulate the model with smaller simulation step [19]. The construction of the co-simulation model can be seen in Fig.15.

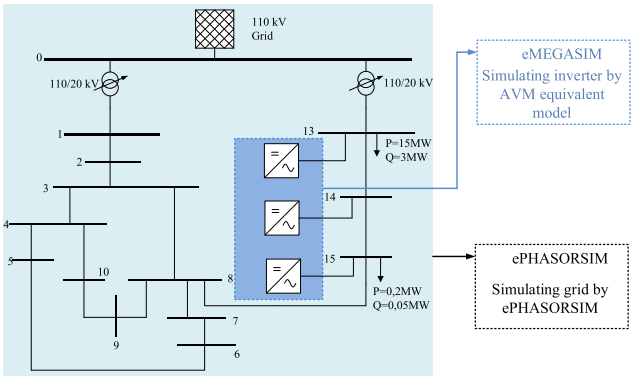

FIGURE 15. Grid topology with two different simulation parts [29].

B. NETWORK REDUCTION

The network reduction is a solution to reduce the simulation time, at the same time the dynamics of the network is substantially emulated [45]–[49]. The procedure of mesh reduction is shown in the following figure. The dynamic behavior of the subordinate and superimposed network is simulated by a transfer function. The transfer function is determined by system identification. The grid reduction is realized using the aggregated model. The behavior of the aggregated model under a small excitation signal is identical to the original system, retaining its main features but changing the structure. After the network reduction, the aggregated models of the subordinate and superimposed networks are integrated with the distribution network instead of using the compact network structures [24]–[26]. This integration model is used for further stability investigation. The aggregated models vary depending on the type of networks to be reduced. The following sections describe two network reduction procedures: the aggregated model for replicating the superimposed or subordinate network.

1) AGGREGATED MODEL TO EMULATE THE OVERLAID NETWORK

The high-voltage grid is often built up as a mesh network to ensure a high level of supply reliability [27], [43], [46]. If the dynamics of the high voltage grid or the interaction of superposed networks must be considered, it is advantageous to use a simplified grid model rather than the compact model to reduce simulation time while maintaining the characteristic dynamics of the superposed network [28]. As part of this work, the high-voltage power network is represented by the aggregated model more precisely by a controlled voltage source, because the behavior of the superposed network from the subordinate network is a non-ideal voltage source. With the aggregated model, both the stationary behavior of the compact model and the dynamic behavior can be modeled.

For this reason, the model is constructed to contain two parts, one of which represents system behavior in steady-state behavior, the other the transient behavior under a small signal. In the aggregated model, the state variables to be considered for the observed phenomenon or the investigation focus can be selected as input or output variables. The inputs denote the operating point while the outputs are the voltage response. The stationary behavior is a measured value that can be calculated by the simulation of the compact network model. The transient behavior can be simulated by a transfer function. The topology of the aggregated model is shown in Fig.16

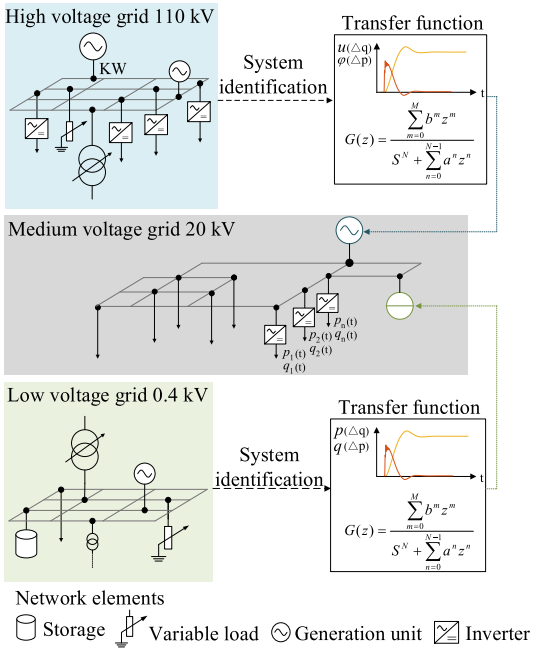

FIGURE 16. Network reduction by employing the aggregated model.

The gray area shows the emulation of the dynamic area and the blue area the emulation of the stationary behavior of the superimposed network. The input signals $\Delta P_{\mathrm{pu}}(t)$ and $\Delta Q_{\mathrm{pu}}(t)$ denotes the temporal operating point change on the medium-voltage network in pu. The use of pu has the advantage that they are relative to a reference and thus identical for the subordinate and superimposed networks. The transfer functions $G_Q(s)$ and $G_P(s)$ and the gain K characterize the dynamic process.

$$G_P(s) = \frac{\Delta\theta_{pu}}{\Delta P}, \quad G_Q(s) = \frac{\Delta u_{pu}}{\Delta Q} \tag{10}$$

The steady-state voltage amplitude U_0 and the steady-state voltage angle θ_0 for the respective phases indicate the stationary behavior of the voltage. After combining the dynamic response and the static output into a complex voltage signal, the voltage source is driven by this voltage signal and the corresponding electrical signal is the output value.

2) AGGREGATED MODEL TO EMULATE THE UNDERLYING GRID

To simulate the subordinate network, a controlled power source model is constructed as an aggregated model. This controlled current source can feed the same active and reactive power as the low-voltage grid into the grid or absorb

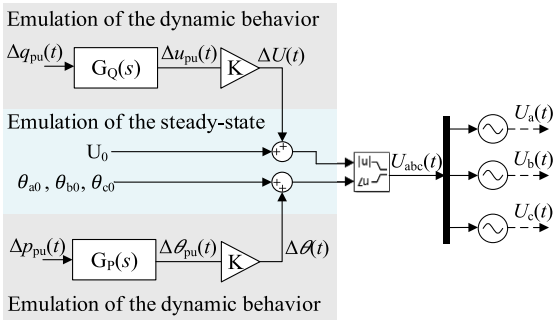

FIGURE 17. Topology of the aggregated model of the overlaid network.

it from the grid. The aggregated model is modeled in two parts: the emulation of dynamic and stationary behavior. The dynamic behavior of the subordinate network is modeled by two transfer functions. The input signal of the transfer functions is the voltage step Δu_{pu} at the superimposed power supply and the output signals are the change of the active and reactive power. The topology is presented in Fig.18.

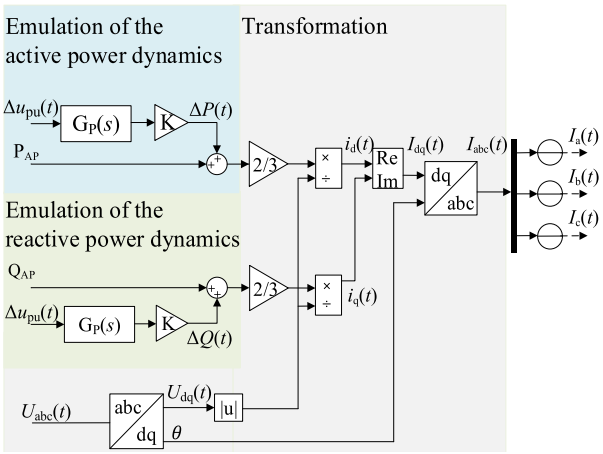

FIGURE 18. Topology of the aggregated model for the emulation of the subordinate network.

The active power and the reactive power dynamics are determined by the composition of the stationary operating points P_{AP} and Q_{AP} by the transfer functions:

$$\mathrm{G_P}(s) = \frac{\Delta P}{\Delta u_{\mathrm{pu}}}, \quad \mathrm{G_Q}(s) = \frac{\Delta Q}{\Delta u_{\mathrm{pu}}} \tag{11}$$

The input signal of the transfer function is the voltage step of the overlaid grid. With the use of the p.u. size, the voltage step can be generated by a high voltage network instead of a voltage source with the same voltage level, whereby the simulation time is reduced. The output signals of the transfer function are the active power ΔP_{pu} and reactive power ΔQ_{pu} response generated by the voltage step. The gain factor K serves, on the one hand, to convert the p.u. values into real values, on the other hand, to adapt the output values when implementing the transfer functions. To build the power source, the active current i_d and the reactive current i_q are calculated by the relationship between active power, reactive power, and voltage and then converted by the inverse-Park transformation into three-phase current signals I_{abc}, see Fig.18

V. EVALUATION

The evaluation of the above methods is illustrated with two indices in this chapter. The focus of the methods is to expand the boundary condition of eMEGASIM to simulate the large-scale power network, the aim of which, accordingly, is to accelerate the simulation speed and it is also called real-time capability [37], [45]. The usage value of core in CPU can correspondingly represent this ability and reflect the simulation consumption. Another essential index is the accuracy of dynamic behavior. By co-simulation and the network reduction, the structure and some parameters of original model are changed. It is crucial to verify that the co-simulation model and the reduced network model does not influence the accuracy of dynamic feature.

A. REAL-TIME CAPABILITY

1) CO-SIMULATION

According to the Fig.15, the basic co-simulation model is constructed with the ePHASORSIM and the AVM of three inverters. The ePHSORSIM simulates the distribution power network based on the Cigré benchmark and the AVM of inverters is simulated by eMEGASIM.

To evaluate its real-time capability, the basic hybrid model, which consists of the 16-buses power grid and three parallel-connected inverters, are initially implemented in real-time simulation, which uses one core in CPU to operate the simulation. TABLE 5 shows the real-time capability of co-simulation model by using one subsystem to execute the simulation.

To investigate the boundary condition of the co-simulation, the simulated number of the inverter is increased until the usage value of core up to 100%. From the table, it can be illustrated that the boundary condition of using eMEGASIM is extended to 9 number of the inverter by co-simulation model, which is 3 inverters by using AVM. With the ARTEMiS DPL (see TABLE 4), the simulation can be indeed accelerated, but the usage of core still reaches 52.88% by using three DPLs. Under the same usage, the co-simulation model can simulate 6 inverters by using AVM.

The extension of the boundary condition using two cores and four cores with the co-simulation is expounded in TABLE 5. The number of simulated inverters can rise to maximal 40 by utilization of more subsystems. In comparison, the maximum simulated number of AVM inverter by eMEGASIM is 10.

It should be noted that the core usage by co-simulation under the same condition, which can be reduced, is because of the ePHASORSIM. In the following table, four real-time simulation scenarios are shown to compare the usage of these models: co-simulation model by using eMEGASIM and

TABLE 5. Real-time capability of co-simulation.

Model	System	Inverter number	Interval [μs]	Usage-value [%]	Running time [μs]
Co-simulation	1	3	50	27.4	13.7
		4		37.2	18.6
		5		48.2	24.1
		6		59.3	29.65
		7		70.2	36
		8		85.9	42.95
		9		98.1	49.05
	2	3	50	12.7	6.35
		4		21.5	10.75
		5		30.3	15.15
		6		38.9	19.45
		7		47.6	23.8
		8		56.6	28.3
		9		65.3	32.65
		19		99.8	49.9
	4	3	50	5.4	2.7
		4		9.7	4.85
		5		15.7	7.85
		6		20.3	10.15
		7		26.8	13.4
		8		32.7	16.35
		9		37.2	18.6
		40		99.89	49.95

ePHASORSIM, AVM by using eMEGASIM, phasor model simulated by eMEGASIM and phasor model simulated by ePHASORSIM.

From the simulation results (TABLE 6), it can be illustrated that the phasor model simulated by ePHASORSIM has the lowest usage with 0.08% by simulating one inverter and 0.1% by simulating three inverters. Because of using ePHASORSIM to simulate the distribution grid in co-simulation model, the usage value, in comparison with AVM, can reduce by about 65%. Another method to extend the boundary condition of simulating more inverters is network reduction, which is illustrated in the next section.

TABLE 6. Comparison of real-time capability of different model under same condition.

Model	System	Inverter number	Interval [μs]	Usage-value [%]	Running time [μs]
Co-simulation	1	1	50	8.45	4.225
		3		27.45	13.73
AVM	1	1	50	75	37.5
		3		90	45
PM	1	1	50	51	25.5
		3		70	352
PM (ePHASORSIM)	1	1	50	0.08	0.04
		3		0.1	0.05

2) NETWORK REDUCTION

Based on network reduction theory in chapter IV, the inverter model can be aggregated as a current source, which is substitute of a transfer function as shown in Fig.19. By system identification, three parallel-connected inverters are aggregated

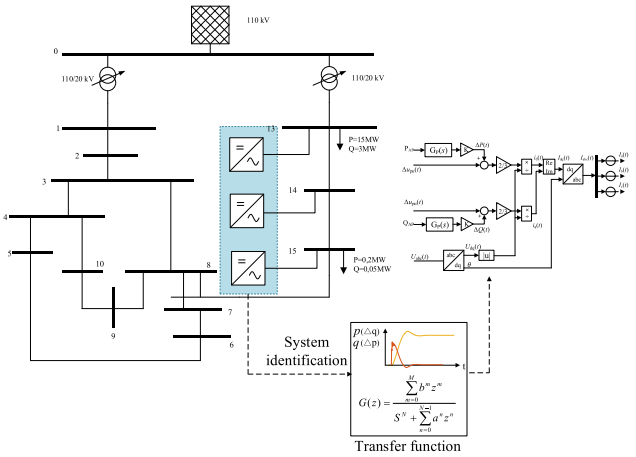

FIGURE 19. Topology of the aggregated model for the emulation of inverters.

to three equivalent current sources. To emulate the inherent dynamic characteristic of an inverter, the function $G_p(s)$ and $G_Q(s)$ are utilized to simulate the response of inverter to the voltage step. The active and reactive power can be feed into a network with I_d and I_q, which are transformed into I_{abc} by using park-transformation [14]. To investigate the influence of interaction between the inverters and the real-time capability of a reduced power network, more inverters are connected parallelly. Every inverter model is reduced to a current source, the dynamic features of them are represented with the transfer function.

The investigation of real-time capability by using network reduction is illustrated in TABLE 7. In this study, there is only one core used to execute the real-time simulation. As is illustrated in table, the usage value of core is 20.8% with three reduced inverter models. The usage doesn't increase significantly with implementation more inverters. With nine reduced inverters, the running time of the whole distribution grid is about 10.5μs, which uses about 21% of the core. To investigate the boundary condition of using one core to execute the real-time simulation by reduced inverter, the number of the inverter is increased till fifty. It is seen that the usage of core grows 5% with increasing ten more reduced inverter models. Because of it, this method is more adaptable to the real-time simulation model with a large amount of inverter, especially for the large-scale power system, when the interaction between the multiple inverters and power system needs to be investigated.

With these two methods, the boundary condition of real-time simulation by eMEGASIM has been exactly extended. According to the context above, the number of simulated AVM inverter can reach a maximum of 40, in comparison with nine without using co-simulation. Another advantage is that the use of ePHASORSIM in co-simulation makes it possible to simulate a large-scale power grid and it has less influence on the real-time capability. As for the network reduction, the inverter model can be substitute by the current

TABLE 7. Real-time capability of aggregated inverter.

Model	Inverter number	Interval [μs]	Usage-value [%]	Running time [μs]
Aggregated inverter model	3	50	20.8	10.4
	4		20.9	10.45
	5		20.9	10.45
	6		21.02	10.51
	7		21.04	10.52
	8		21.6	10.8
	9		21.08	10.54
	20		25.1	12.55
	30		30.2	15.1
	40		35.8	17.9
	50		40.1	20.05

source, which is represented through a character transfer function. With this method, the number of inverters implemented in real-time simulation can reach a maximum pf over one hundred.

As mentioned above, the structure of the harmonic source from DC link of the inverter is simplified to reduce the computation time of the simulation. To emulate the influence of the oscillation in the switching process from inverter, the current source shown in Fig.19 is not able to satisfy the requirements.

The main source of oscillation in power grid is the harmonic. Therefore, the harmonics from the DC link in the inverter need to be considered in the aggregated model. In the traditional harmonic analysis, the harmonic generator is considered as an ideal current source [50]. The single-phase Norton-equivalent model for simulating the harmonic by current source is shown in Fig.20. The harmonic current is modelled by parallel connection of a current source $I_{N,h}$ and a harmonic impedance $Z_{N,h}$. To consider the effects of oscillations in the inverter on the power grid, the aggregated current source is configurated as in Fig.21.

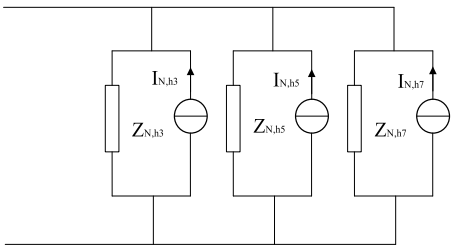

FIGURE 20. Single-phase Norton-equivalent model [50].

The dynamic feature of the inverter is emulated by the function $G_p(s)$ and $G_Q(s)$. The oscillation in inverter is simulated with the harmonic source. The investigation of real-time capability in the aggregated inverter model with the harmonic source is operated with the same scenario in TABLE 8. The results in TABLE 8 illustrate that the aggregated model of the inverter with harmonic source has a higher usage of core. In the account of the low-frequency oscillation and high-frequency oscillation from the inverter, the current source

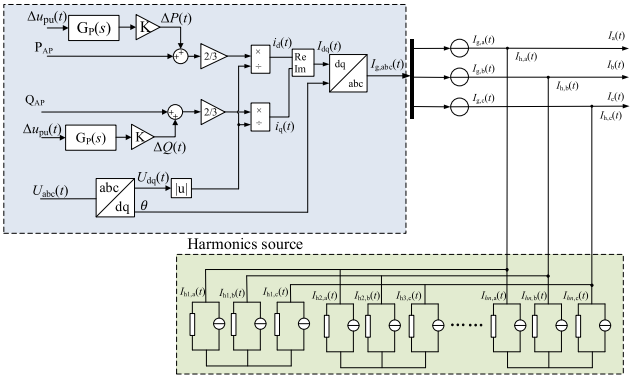

FIGURE 21. Topology of the aggregated model for the emulation of inverters with harmonic source.

TABLE 8. Real-time capability of aggregated inverter with harmonic source.

Model	Inverter number	Interval [μs]	Usage-value [%]	Running time [μs]
Aggregated inverter model with harmonic source	3	50	21.5	10.75
	4		22.1	11.05
	5		23.2	11.6
	6		24.01	12.005
	7		25.2	12.6
	8		27.3	13.65
	9		28.8	14.40
	20		32.2	16.10
	30		37.3	18.65
	40		43.8	21.9
	50		50.1	25.05

with 5 Hz, 15Hz, 25Hz,150Hz, 250Hz harmonic source are combined in the aggregated inverter model. In comparison with the TABLE 7, the usage of core with 50 aggregated inverter model considered the oscillation is about 5% higher than without consideration of the oscillation influence, the running time of which is 25.05μs.

According to the results, the co-simulation and the network reduction are able to improve the calculation performance in real-time simulation. Without these two methods, the maximum simulated inverter number in DEM type is 4 and in AVM type is 10 with implementation of parallel computing. With the two methods, this boundary condition is extended to 40 AVM inverters by co-simulation and 100 inverters emulated by current source with harmonic source with consideration of oscillation. Except for the extension the boundary condition of eMEGASIM, there is another problem needed to be considered whether the difference between the new model and original one is enlarged. In next section, the dynamic behavior of new models built by co-simulation and network reduction and the original AVM model is observed to compare the difference between them.

B. THE SIMILARITY BY CO-SIMULATION AND NETWORK REDUCTION

In this section, the investigation of difference between the model built by co-simulation and network reduction and the

original AVM is studied to verify that the dynamic behavior of new model is similar with the original. Based on this condition, the new model can be implemented to replace the AVM model, which is to simulate the large-scale power grid with many inverters.

1) CO-SIMULATION

The verification of model built by co-simulation is through observing the dynamics of distribution grid by changing the operating point of the inverter. The dynamic behavior of current change at the point of common coupling (PCC) is illustrated in Fig.22.

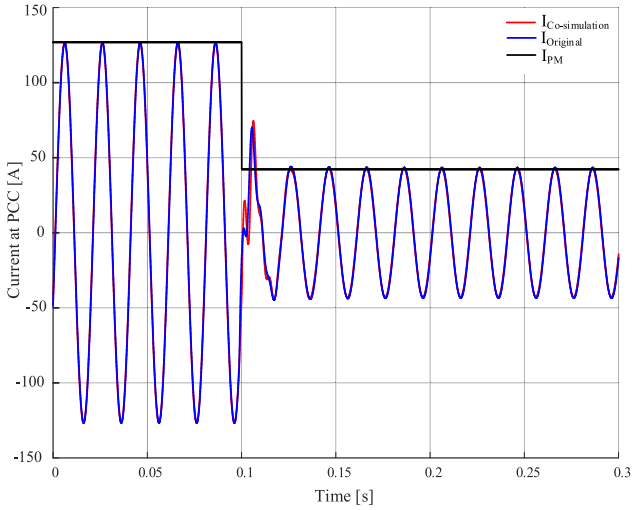

FIGURE 22. Current behavior at the PCC by co-simulation.

It is shown that the stationary behavior at PCC has only relatively small deviations from 0s to about 0.1s and from 0.13s to 0.3s. Meanwhile, there is a small deviation in the dynamic swinging. Especially, the sharp point of the first swing from the co-simulation model reaches about 25 A, which is about 2 A from the original AVM. As for the dynamic process simulated directly by ePHASORSIM, which is presented by the black curve, the dynamic process has been neglected with setting the simulation period as 0.02s. It is nearly the smallest simulation step that ePHASORSIM can be set.

To quantify the similarity between both models, the TABLE 9 compares the peak value, overshoot, rising time, and the settling time of dynamic transient. From the above figure, there are two peaks during the transient process (see red and blue curve). The first of them is more deviated in comparison with the second peak. The following table describes the values of the second peak, which shows that peak value of the original model is 68A, while the model built by co-simulation is 71.8A. The fitting of both values reaches 91.47%. As for the overshoot, the original model is 25A and the co-simulation is 3.8A more than the original one, the fitting of which has about 14% difference.

Another criterion to evaluate the fitting degree of both models is the rise time. It means the time consumption from

TABLE 9. Evaluation of dynamic similarity of current state in co-simulation.

	Original model	Co-simulation	Fit
Peak value [A]	68	71.8	94.71%
Overshoot [A]	25	28.8	86.89%
Rise time [s]	0.011	0.0111	98.18%
Settling time [s]	0.019	0.0192	98.95%

the start point of operation state-changing until the peak value. As the illustration in the table, the original model and co-simulation model takes separately 0.011s and 0.0111s from the change point to the peak value in transient procedure. The last indicator is the settling time, which implies the time consumption from the changing point to the next stationary state.

The difference between both models on the settling time is 0.002s. Hence, the fitting of two models can reach to 98.95%. According to the fitting values (see TABLE 9), it is illustrated that the dynamic behavior of current from co-simulation model has a high similarity with the original model.

Except for the current dynamic, the active and reactive power at PCC is observed to evaluate the similarity between both models.

Fig.23 shows the dynamic character by changing the operating point of inverter. From the perspective of the static condition, the performance of the co-simulation model and the AVM is nearly the same (see blue and red line). There is no deviation between them from 0s to 0.1s and from 0.2s to 0.3s. During the transient procedure, it can be observed that the dynamic of active power has a smaller deviation than the reactive power. The similarity of dynamic from reactive and active power is higher than the current. TABLE 10 illustrates the fitting values according to the four evaluation indexes to

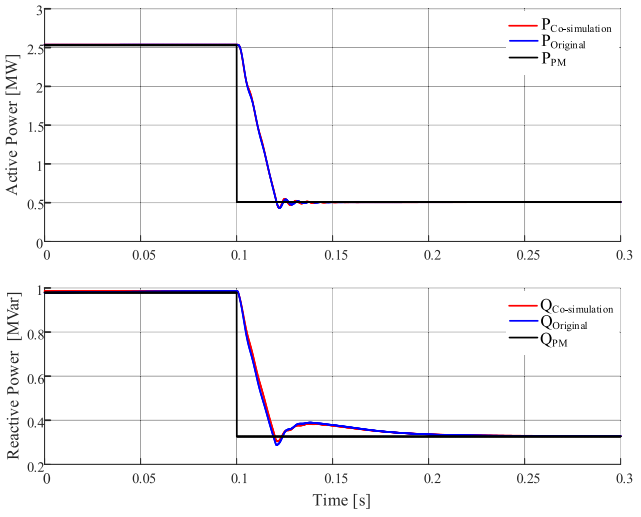

FIGURE 23. Behavior of active and reactive power at PCC by co-simulation.

TABLE 10. Evaluation of dynamic similarity of power state in co-simulation.

	Original model	Co-simulation	Fit
Peak value P [MW]	0.435	0.4349	99.97%
Peak value Q [MVar]	0.316	0.309	97.78%
Overshoot P [MW]	2.065	2.0651	99.99%
Overshoot Q [MVar]	0.684	0.691	98.98%
Rise time [s]	0.011	0.0111	98.18%
Settling time P [s]	0.043	0.0429	99.76%
Settling time Q [s]	0.12	0.124	96.77%

TABLE 11. Evaluation of dynamic similarity of power states in aggregated model.

	Original model	Reduced model	Fit
Peak value P [MW]	5.79	5.81	99.65%
Peak value Q [MVar]	2.883	2.890	99.75%
Overshoot P [MW]	1.04	1.06	98.07%
Overshoot Q [MVar]	1.447	1.454	99.52%
Rise time [s]	0.067	0.065	97.01%
Settling time P [s]	0.251	0.253	99.20%
Settling time Q [s]	0.647	0.645	99.69%

quantify the similarity of the dynamics of active and reactive power between both models. In the transient procedure, the active power and reactive power have the synchronous rising time in both models. The fitting of rising time in both models is over 98%, which has high similarity. As for the other values like the peak value, overshoot and settling time, the dynamic behavior of active power has a higher similarity degree than the reactive power. The fitting values of active power are almost over 99%, while these values of reactive power are all around from 96% to 98%.

According to the context and tables above, it can be illustrated that the dynamic behavior of model built by co-simulation has a high similarity with the original model, which means that the co-simulation can be utilized to build the substitute models to simulate the large-scale power system. In the next section, the same investigation is implemented to evaluate the model built by network reduction.

2) NETWORK REDUCTION

To verify the similarity between the original model and the model built by network reduction, the dynamics at PCC between the reduced inverter and distribution grid are observed. Fig.24 illustrates the dynamic movements of active and reactive power in distribution grid when the 110kV level changes $\Delta U = 0.1$p.u. Without changing the operation point of inverter, the total injected power from inverter is invariant despite the change of the voltage at 110kV level.

TABLE 11 summarizes and compares the dynamic values of active and reactive power in the distribution grid for original and reduced model. The peak value of active power in both models has 0.02MW deviation. The fitting degree of reduced model to the original model can reach 99.65%. Similarly, the peak value of reactive power between the models has a high fitting, which is also over 99%. As for the other

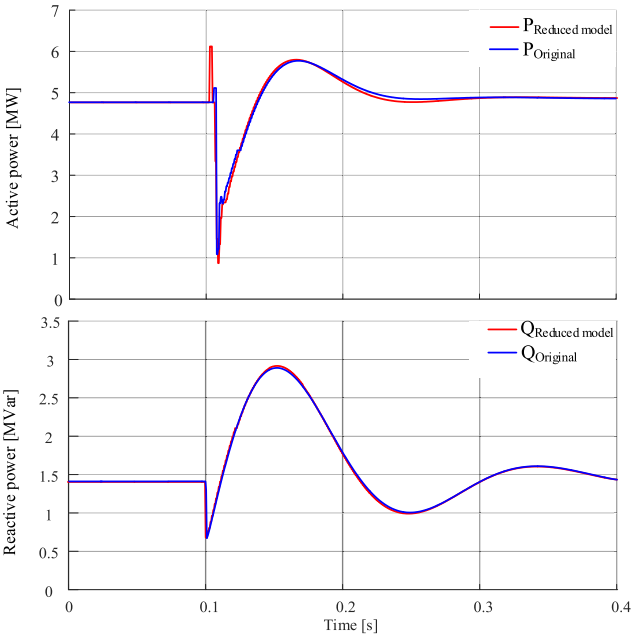

FIGURE 24. Behavior of active and reactive power at PCC by network reduction.

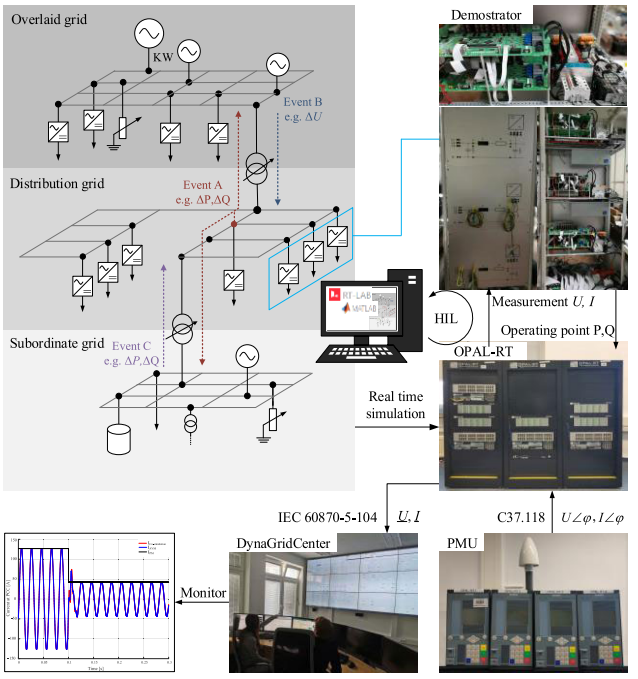

FIGURE 25. Application of OPAL-RT in HIL and DynaGridCenter [51].

evaluation values like the overshoot, rise time and settling time, the fitting values of them can all reach beyond 97%.

As illustrated in this section, the dynamic behavior of active and reactive power from the reduced model has a high similarity with the original model. It can be observed that, except for the obvious deviation direct after the operation point change in the curve of active power, the most parts of curves of active and reactive power for both models are run-

ning similarly. All the values for the evaluation of the fitting degree between the reduced model and the original model are over 97%. Accordingly, the model built by network reduction is applicable in modeling the large-scale power network with many distribution generations through inverters.

VI. CONCLUSION AND OUTLOOK

In this paper, two methods are proposed to improve the performance of the real-time simulation. Nowadays, the large-scale power grid with distributed generation is more indeed to be simulated because of the developing of renewable power generation and the enlarging of the power grid. The traditional simulation cannot succeed in simulating the large-scale power grid with many inverter models because of the burdensome numerical calculation. Because of the powerful calculation ability of real-time simulator, it is increasingly applied to the complex and the large-scale power grid simulation.

Without the implementation of the proposed methods, the number of simulated inverters is limited. As illustrated above, the maximal simulated number of inverters without acceleration methods can only be four by DEM and AVM. With the acceleration methods like the parallel computing and the ARTEMiS block, the boundary condition can be extended to ten as the maximal simulated number of inverters, which is far beyond the requirement for the large-scale power grid.

By co-simulation, the power grid model is divided into two parts: the transmission grid and the distributed inverter-based generations. These two parts use model types in different deep levels. With the utilization of ePHASORSIM in co-simulation, the complexity of the model is effectively reduced. According to the investigation results, the boundary condition, by using one core of the simulator, can be extended to nine AVM inverter models as the maximal simulated number of inverters. With parallel computing by using four cores, the maximal simulated number of inverters can reach up to forty, which is three times more than the simulation without using co-simulation. In comparison with the original model, the co-simulation model is about over 95% similar to it. Likewise, the similarity between the original model and model built by network reduction is also investigated. The results show that the dynamics of the two models have an average of over 97% similarity. The boundary condition with one core for the real-time simulation can to be extended to one hundred inverter models as the maximal simulated number. With the above two methods, a large-scale power grid with inverter-dominated generations can be modeled and applied to investigate the interaction between the inverter and the power grid through the intranet and internet in the future. For the sake of improving the reliability of simulation, the part of the model can be substituted by the demonstrator with the HIL simulation, see Fig.25. The large-scale power grid with the amount of inverter-based generations and loads are simulated in the real-time simulator by the methods proposed in this paper to improve the performance of the real-time simulation.

REFERENCES

[1] Q. Zhong and T. Hornik, *Control of Power Inverters in Renewable Energy*. Hoboken, NJ, USA: Wiley, Feb. 2010.

[2] R. Teodorescu, M. Liserre, and P. Rodriguez, *Grid Converters for Photovoltaic and Wind Power Systems*. Hoboken, NJ, USA: Wiley, Feb. 2011.

[3] G. Putrus, J. Wijayakulasooriya, and P. Minns, "Power quality: Overview and monitoring," in *Proc. Int. Conf. Ind. Inf. Syst.*, 2007, pp. 551–558.

[4] X. Chen and J. Sun, "Characterization of inverter-grid interactions using a hardware-in-the-loop system test-bed," in *Proc. 8th Int. Conf. Power Electron. (ECCE Asia)*, May 2011, pp. 2180–2187.

[5] J. Elizondo and J. L. Kirtley, "Effect of inverter-based DG penetration and control in hybrid microgrid dynamics and stability," in *Proc. Power Energy Conf. Illinois (PECI)*, Feb. 2014, pp. 1–6.

[6] J. Fortmann, S. Engelhardt, J. Kretschmann, C. Feltes, and I. Erlich, "New generic model of DFG-based wind turbines for RMS-type simulation," *IEEE Trans. Energy Convers.*, vol. 29, no. 1, pp. 110–118, Mar. 2014.

[7] *Guide for the Develpment of Models for HVDC Converters in a HVDC Grid*, CIGRE, Working Group B4. 57, 2014

[8] V. J. Thottuvelil, D. Chin, and G. C. Verghese, "Hierarchical approaches to modeling high-power-factor AC-DC converters," *IEEE Trans. Power Electron.*, vol. 6, no. 2, pp. 179–187, Apr. 1991.

[9] N. Mohan, W. P. Robbins, T. M. Undeland, and R. Nilssen, "Simulation of power electronic and motion control systems—An overview," *Proc. IEEE*, vol. 82, no. 8, pp. 1287–1302, Aug. 1994.

[10] T. Yang, "Development of dynamic phasors for the modeling of aircraft electrical power systems," Ph.D. dissertation, Dept. Elect. Electron. Eng., Univ. Nottingham, Nottingham, U.K., 2013.

[11] T. Demiray, "Simulation of power system dynamics using dynamic phasor models," Ph.D. dissertation, Swiss Federal Inst. Technol. Zurich, Zürich, Switzerland, 2008.

[12] S. Chiniforoosh, J. Jatskevich, A. Yazdani, V. Sood, V. Dinavahi, J. A. Martinez, and A. Ramirez, "Definitions and applications of dynamic average models for analysis of power systems," *IEEE Trans. Power Del.*, vol. 25, no. 4, pp. 2655–2669, Oct. 2010.

[13] B. Lehman and R. M. Bass, "Switching frequency dependent averaged models for PWM DC-DC converters," *IEEE Trans. Power Electron.*, vol. 11, no. 1, pp. 89–98, Jan. 1996.

[14] *Benchmark Systems for Network Integration of Renewable and Distributed Energy Resources*, CIGRE, document TF C6.04.02, 2010.

[15] T. Berry, A. R. Daniels, and R. W. Dunn, "Real time simulation of power system transient behaviour," in *Proc. 3rd Int. Conf. Power Syst. Monit. Control*, London, U.K., Jun. 1991, pp. 122–127.

[16] P. M. Menghal and A. J. Laxmi, "Real time simulation: Recent progress & challenges," in *Proc. Int. Conf. Power, Signals, Controls Comput. (EPSCICON)*, Thrissur, India, Jan. 2012, pp. 1–6.

[17] A. Dubey, S. Chakrabarti, and V. Terzija, "Testing and validation of a dynamic estimator of states in OPAL-RT real time simulator," in *Proc. IEEE Power Energy Soc. Gen. Meeting*, Chicago, IL, USA, Jul. 2017, pp. 1–5.

[18] X. Guillaud, M. O. Faruque, A. Teninge, A. H. Hariri, L. Vanfretti, M. Paolone, V. Dinavahi, P. Mitra, G. Lauss, C. Dufour, P. Forsyth, A. K. Srivastava, K. Strunz, T. Strasser, and A. Davoudi, "Applications of real-time simulation technologies in power and energy systems," *IEEE Power Energy Technol. Syst. J.*, vol. 2, no. 3, pp. 103–115, Sep. 2015.

[19] S. Kumaravel, R. S. Narayan, T. O'Donnell, and C. O'Loughlin, "Genetic algorithm based PI tuning of VSC-HVDC system and implementation using OPAL-RT," in *Proc. IEEE Region 10 Conf. (TENCON)*, Penang, Malaysia, Nov. 2017, pp. 2193–2197.

[20] F. Plumier, C. Geuzaine, and T. Van Cutsem, "A multirate approach to combine electromagnetic transients and fundamental-frequency simulations," in *Proc. Int. Conf. Power Syst. Transients*, 2013, pp. 1–7.

[21] F. J. Plumier, C. Geuzaine, and T. Van Cutsem, "On the convergence of relaxation schemes to couple phasor-mode and electromagnetic transients simulations," in *Proc. IEEE PES Gen. Meeting|Conf. Expo.*, Jul. 2014, pp. 1–5.

[22] D. Z. Fang, W. Liwei, T. S. Chung, and K. P. Wong, "New techniques for enhancing accuracy of EMTP/TSP hybrid simulation," *Int. J. Elect. Power Energy Syst.*, vol. 28, pp. 707–711, Dec. 2006.

[23] G. W. J. Anderson, "Hybrid simulation of AC-DC power systems," Ph.D. dissertation, Univ. Canterbury, Christchurch, New Zealand, 1995.

[24] J. B. Ward, "Equivalent circuits for power-flow studies," *Elect. Eng.*, vol. 68, no. 9, p. 794, Sep. 1949.

[25] J. Mahseredjian, S. Dennetière, L. Dubé, B. Khodabakhchian, and L. Gérin-Lajoie, "On a new approach for the simulation of transients in power systems," *Electr. Power Syst. Res.*, vol. 77, no. 11, pp. 1514–1520, Sep. 2007.
[26] A. A. van der Meer, M. Gibescu, M. A. M. M. van der Meijden, W. L. Kling, and J. A. Ferreira, "Advanced hybrid transient stability and EMT simulation for VSC-HVDC systems," *IEEE Trans. Power Del.*, vol. 30, no. 3, pp. 1057–1066, Jun. 2015.
[27] J. Beerten, O. Gomis-Bellmunt, X. Guillaud, J. Rimez, A. van der Meer, and D. Van Hertem, "Modeling and control of HVDC grids: A key challenge for the future power system," in *Proc. Power Syst. Comput. Conf.*, Aug. 2014, pp. 1–21.
[28] X. Mao and R. Ayyanar, "Average and phasor models of single phase PV generators for analysis and simulation of large power distribution systems," in *Proc. 24th Annu. IEEE Appl. Power Electron. Conf. Expo.*, Feb. 2009, pp. 1964–1970.
[29] Cigre WG B4-57, "Guide for the development of models for HVDC converters in a HVDC grid," WG Brochure, 2014.
[30] M. Foley, Y. Chen, and A. Bose, "A real time power system simulation laboratory environment," *IEEE Trans. Power Syst.*, vol. 5, no. 4, pp. 1400–1406, Nov. 1990.
[31] O. Devaux, L. Levacher, and O. Huet, "An advanced and powerful real-time digital transient network analyser," *IEEE Trans. Power Del.*, vol. 13, no. 2, pp. 421–426, Apr. 1998.
[32] H. Taoka, I. Iyoda, H. Noguchi, N. Sato, and T. Nakazawa, "Real-time digital simulator for power system analysis on a hypercube computer," *IEEE Trans. Power Syst.*, vol. 7, no. 1, pp. 1–10, Feb. 1992.
[33] I. Etxeberria-Otadui, V. Manzo, S. Bacha, and F. Baltes, "Generalized average modelling of FACTS for real time simulation in ARENE," in *Proc. IEEE 28th Annu. Conf. Ind. Electron. Soc. (IECON)*, vol. 2, Nov. 2002, pp. 864–869.
[34] M. O. Faruque and V. Dinavahi, "An advanced PC-cluster based real-time simulator for power electronics and drives," in *Proc. IEEE Int. Symp. Ind. Electron.*, Montreal, QC, Canada, Jul. 2006, pp. 2579–2584.
[35] C. Larose, S. Guerette, F. Guay, A. Nolet, T. Yamamoto, H. Enomoto, Y. Kono, Y. Hasegawa, and H. Taoka, "A fully digital real-time power system simulator based on PC-cluster," *Math. Comput. Simul.*, vol. 63, nos. 3–5, pp. 151–159, Nov. 2003.
[36] G. Sybille and P. Giroux, "Simulation of FACTS controllers using the MATLAB power system blockset and hypersim real-time simulator," in *Proc. IEEE Power Eng. Soc. Winter Meeting. Conf.*, vol. 1, New York, NY, USA, Jan. 2002, pp. 488–491.
[37] M. Steurer, C. S. Edrington, M. Sloderbeck, W. Ren, and J. Langston, "A megawatt-scale power hardware-in-the-loop simulation setup for motor drives," *IEEE Trans. Ind. Electron.*, vol. 57, no. 4, pp. 1254–1260, Apr. 2010.
[38] D. Jakominich, R. Krebs, D. Retzmann, and A. Kumar, "Real time digital power system simulator design considerations and relay performance evaluation," *IEEE Trans. Power Del.*, vol. 14, no. 3, pp. 773–781, Jul. 1999.
[39] M. Kezunovic, J. Domaszewicz, V. Skendzic, M. Aganagic, J. K. Bladow, S. M. McKenna, and D. M. Hamai, "Design, implementation and validation of a real-time digital simulator for protection relay testing," *IEEE Trans. Power Del.*, vol. 11, no. 1, pp. 158–164, Jan. 1996.
[40] X. Wang and R. M. Mathur, "Real-time digital simulator of the electromagnetic transients of transmission lines with frequency dependence," *IEEE Trans. Power Del.*, vol. 4, no. 4, pp. 2249–2255, Oct. 1989.
[41] F. Guay, J. Cardinal, E. Lemiex, and S. Guerette, "Digital real-time simulator using IEC 61850 communication for testing devices," in *Proc. CIGRE Canada Conf.*, Montreal, QC, Canada, Sep. 2012, pp. 1–7.
[42] T. J. Member, S. Xinya, J. Willkomm, S. Schlegel, and D. Westermann, "Hybrids-simulation using EMT–and phasor-based model for converter dominated distribution grid," in *Proc. IEEE PES Innov. Smart Grid Technol. Conf. Eur. (ISGT-Eur.)*, Sarajevo, Bosnia and Herzegovina, Oct. 2018, pp. 1–6.
[43] S. Deckmann, A. Pizzolante, A. Monticelli, B. Stott, and O. Alsac, "Numerical testing of power system load flow equivalents," *IEEE Trans. Power App. Syst.*, vol. PAS-99, no. 6, pp. 2292–2300, Nov. 1980.
[44] S. C. Savulescu, "Equivalents for security analysis of power systems," *IEEE Trans. Power App. Syst.*, vol. PAS-100, no. 5, pp. 2672–2682, May 1981.
[45] S. C. Savulescu, *Real-time Stability Assessment in Modern Power System Control Centers*, vol. 42. Hoboken, NJ, USA: Wiley, 2009.
[46] J. Machowski, A. Cichy, F. Gubina, and P. Omahen, "External subsystem equivalent model for steady-state and dynamic security assessment," *IEEE Trans. Power Syst.*, vol. 3, no. 4, pp. 1456–1463, Nov. 1988.
[47] J. P. Yang, G. H. Cheng, and Z. Xu, "Dynamic reduction of large power system in PSS/E," in *Proc. IEEE/PES Transmiss. Distrib. Conf. Expo. Asia Pacific*, Aug. 2005, pp. 1–4.
[48] M. Vardikar, S. Chakrabarti, and E. Kyriakides, "Transformation of measurements for using external network equivalents in state estimation," in *Proc. IEEE Power Energy Soc. Gen. Meeting*, Jul. 2013, pp. 1–5.
[49] K. Dongare, S. Chakrabarti, and E. Kyriakides, "Power system state estimation considering real-time equivalents of the external networks," in *Proc. IEEE Innov. Smart Grid Technol.-Asia (ISGT Asia)*, Nov. 2013, pp. 1–6.
[50] E. Thunberg and L. Soder, "A harmonic Norton model of a real distribution network," in *Proc. 8th Int. Conf. Harmon. Qual. Power.*, Athens, Greece, Oct. 1998, pp. 279–284.
[51] E. Glende, P. Trojan, I. Hauer, A. Naumann, C. Brosinsky, M. Wolter, and D. Westermann, "Communication infrastructure for dynamic grid control center with a hardware-in-the-loop model," in *Proc. IEEE PES Innov. Smart Grid Technol. Conf. Eur. (ISGT-Eur.)*, Sarajevo, Bosnia Herzegovina, Oct. 2018, pp. 1–6.

XINYA SONG (Member, IEEE) received the M.Sc. degree in electrical power and control engineering from the Technische Universität Ilmenau, Germany, in 2018. He has been a Research Fellow of the Power Systems Group, Technische Universität Ilmenau, since 2018. His main research interests include the control and modeling of future distribution networks with a particular interest in dynamic investigations and the simulation of models in the real-time simulator.

HUI CAI (Member, IEEE) received the M.Sc. degree in electrical power and control engineering from Technische Universität Ilmenau, Germany, in 2019. She joined the Power Systems Group, Technische Universität Ilmenau, in 2019, as a Research Fellow. Her main research interests include the design, control, modeling, and operation of the HVDC power systems and the simulation of models in the real-time simulator.

TENG JIANG (Member, IEEE) received the bachelor's degree in business administration from the North China University of Technology in 2002, and the bachelor's degree in mechanical engineering and the M.Eng. degree in electrical power control engineering from Technische Universität Ilmenau in 2012, where he is currently pursuing the Ph.D. degree with the Power Systems Group. His research interests include power system modeling and simulation as well as distribution grid operation.

TOM SENNEWALD (Member, IEEE) received the M.Sc. degree in electrical power and control engineering from Technische Universität Ilmenau, Germany. In the same year, he joined the Power Systems Group, Technische Universität Ilmenau, as a Research Fellow. His main research interests include the design, control, modeling, and operation of future power systems with a particular interest in the optimization of HVDC grids.

JAN KIRCHEIS (Student Member, IEEE) received the B.Eng. degree in electrical engineering from the Bielefeld University of Applied Sciences in 2017. He is currently pursuing the master's degree in electrical power and control engineering with the Technische Universität Ilmenau, Germany. His main research interests include inverter dominated grids, with the emphasis of modeling and controlling power grids.

STEFFEN SCHLEGEL (Member, IEEE) received the Ph.D. degree in electrical engineering from Technische Universität Ilmenau in 2015. He held a postdoctoral position at Technische Universität Ilmenau, where he is a Chief Engineer and the Head of the Research Team ''Vertical System Operation'' at the Power Systems Group. His research interests include the system integration of transmission and distribution grid operation, and new power system operation methodologies with an active interface between distribution and transmission grid operators.

LEONEL NORIS MARTINEZ (Member, IEEE) was born in Celaya, Mexico, in 1990. He received the B.S. degree in electromechanical engineering from the Monterrey Institute of Technology and Higher Education (ITESM), in 2013, and the M.S. degree in electrical power engineering from the Delft University of Technology (TU Delft), in 2018.

From 2013 to 2014, he was a Research Assistant with the Schneider-Electric MDIC Centre. From 2014 to 2016, he was an Engineer with ABB. During the M.S. degree studies, he did an internship in the Dutch TSO TenneT, where he translated a Type-3 WF model designed in the PSCAD to RTDS. He currently collaborates with Opal-RT Technologies as a Field Application Engineer. His research interests include renewable energy, the modeling and analysis of restoration of power systems with high penetration of power electronic converters, the dynamic simulation of power grids, the modeling of control systems, HVDC, BESS, and power system protection.

YOUCEF BENZETTA was born in Algeria, in 1984. He received the M.E. degree from the Ecole Polytechnique of Algiers, Algeria, in 2008, and the M.E. degree from Grenoble INP, France, in 2017. He joined CEEG-Sonelgaz Alger, in 2009, as a Contracts Engineer/Site Project Manager of several turnkeys' contracts for combined cycle/simple cycle power plants projects. Since 2018, he has been with OPAL-RT Technologies, where he is currently an Application Engineer. His main interests include real-time simulation solutions, including software and hardware, designing and validating complex electrical systems, and the control structures associated thanks to hardware-in-the-loop and rapid control prototyping applications. As a member of the technical team, he is directly involved in research and development projects, especially in the electrical grid and the power conversion fields. His customers belong to the industrial world, such as ABB, Alstom, EDF, EADS, Delphi, DCNS, General Electric, Renault, and SAFRAN, as well as renowned research laboratories.

DIRK WESTERMANN (Senior Member, IEEE) received the Dipl.Ing. and Dr.Ing. degrees from the University of Dortmund, Germany.

In 1997, he joined ABB Ltd., Zurich, Switzerland, where he held several positions in Research and Development and technology management. In 2005, he became the Director of the Institute of Electrical Power and Control Technologies, Technische Universität Ilmenau. Since 2019, he has been responsible for the Center of Energy Technology and the Institute for Energy, Drive, and Environmental Systems Technology. His current research interests include power system operation and design with special attention to HVDC grids, system operation in the light of 100% renewables, new architectures of power system control systems, and assistance systems for better asset utilization.